RESEARCH ARTICLE

Macromolecular Materials and Engineering
Open Access
www.mame-journal.de

# Light-Driven Structural Detachment and Controlled Release in Smart Antibacterial Multilayer Platforms

*Zuzanna J. Krysiak, Daniel Rybak, Tetuko Kurniawan, Anna Zakrzewska, and Filippo Pierini**

**Smart materials, especially light-responsive, have become a key research area due to their tunable properties. It is related to the ability to undergo physical or chemical changes in response to external stimuli. Among them, photothermal responsive materials have attracted great interest. This study focuses on the development of a multilayer system (MS) consisting of benzophenone-modified polydimethylsiloxane (PDMS) ring and a thermo-responsive core made of poly(N-isopropylacrylamide-co-N-isopropylomethacrylamide) (P(NIPAAm-*co*-NIPMAAm)), gelatin, and gelatin methacrylate (GelMA). The system utilizes the thermal sensitivity of P(NIPAAm-*co*-NIPMAAm) and the photothermal effect of gold nanorods (AuNRs) to achieve an on-demand controlled release mechanism within 6 min of near-infrared (NIR) light irradiation. The mechanical properties investigated in the compression test show significant improvement in MS, reaching 60 times greater value than the material without a PDMS ring. In addition, NIR irradiation for 15 min activated the antimicrobial properties, eliminating 99.9% of *E. Coli* and 100% of *S. Aureus*, thus presenting pathogen eradication. This platform provides a versatile methodology for developing next-generation smart materials, advanced delivery mechanisms, and multifunctional nanostructured composites. This work highlights the potential of photosensitive materials to revolutionize the field of soft robotics, optics and actuators, and on-demand systems by providing precise control over release dynamics and improved material properties.**

## 1. Introduction

For a few decades, the field of smart materials has seen extreme growth, and new solutions are being sought.[1] Stimuli-responsive materials attract the most attention as they undergo physical/chemical modification when exposed to external stimuli.[2] Heat, light,[3] pH,[4,5] electricity,[6] and mechanical stress[7] are used to induce the desired action in the smart materials. These tunable properties benefit many applications, such as actuators, sensors,[8] smart textiles,[9] and biomedical materials.[10] Smart materials are fabricated mainly based on polymers, hydrogels,[11] and carbon-based components.[12,13]

Hydrogels are easy-to-process, 3D networks with great porosity,[14] enabling the bonding of molecules within the hydrogel matrix.[15,16] Among many hydrogels, the group of thermo-sensitive is commonly reported on the topic of smart materials.[17] The response phenomena are related to the volume phase transition temperature (VPTT) in which the phase separation occurs above the critical temperature.[5,18,19] Poly(N-isopropylacrylamide) (PNIPAAm), frequently used for smart hydrogel manufacturing, has VPTT at ≈32 °C.[20,21] The hydrogel matrix shrinks above this temperature, changing properties from hydrophilic to hydrophobic. It is attributed to the rearrangement of hydrogen bonds, which is reversible; the formation of inter- and intrachain hydrogen bonds between the amide groups occurs as the water-polymer bonds are broken.[22] The critical temperature can be shifted by blending PNIPAAm with other polymers. For instance, copolymerization with poly(N-isopropylomethylacrylamide) (PNIPMAAm) with VPTT ≈42 °C leads to the VPTT increase to ≈33–34 °C.[23,24] To facilitate the application of the thermal sensitivity of hydrogels, plasmonic particles are incorporated into the bulk of the material to induce cascade stimuli response behavior.[25,26] The gold nanoparticles irradiated with light with a dedicated wavelength activate the surface plasmon resonance (SPR).[27] Therefore, the NIR light is converted into local heat and triggers the thermal response of the hydrogel.[28] The physical changes in the hydrogel matrix are generated, affecting its mechanical properties.[29–32]

Z. J. Krysiak, D. Rybak, T. Kurniawan, A. Zakrzewska, F. Pierini
Department of Biosystems and Soft Matter
Institute of Fundamental Technological Research
Polish Academy of Sciences
Warsaw 02-106, Poland
E-mail: fpierni@ippt.pan.pl
T. Kurniawan
President University
Jl. Ki Hajar Dewantara, Kota Jababeka, Bekasi 17550, Indonesia

The ORCID identification number(s) for the author(s) of this article can be found under https://doi.org/10.1002/mame.202400462



**DOI: 10.1002/mame.202400462**

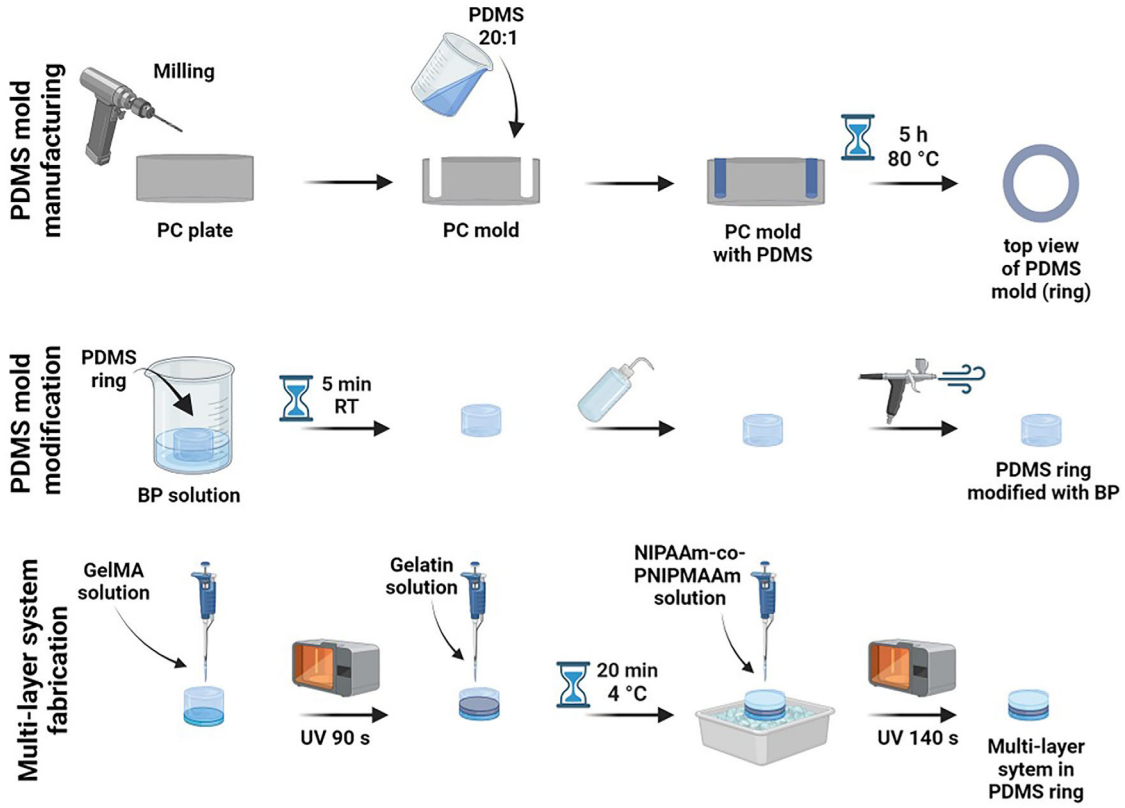


**Figure 1.** The step-by-step preparation scheme presents PDMS mold manufacturing, PDMS mold modification, and MS fabrication.

The search for new strategies in on-demand systems is essential due to its potential to revolutionize the smart materials market.[33,34] Innovative materials can provide superior mechanical properties or more precise release mechanisms.[35,36] Thermo-responsive materials are already broadly used in on-demand release systems,[37] particularly drug delivery materials. These systems operate by rearranging the material's bulk structure in response to external stimuli, enabling the controlled release of drugs encapsulated within hydrogels according to specific needs.[38,39] However, current release systems are based on small molecule/drug entrapment, thus lacking the possibility to release a greater part of the manufactured system[40,41] and be applied as soft robotics, actuators, or optics.[42]

In this study, we developed a multilayer system (MS) consisting of a polydimethylsiloxane (PDMS) ring modified with benzophenone (BP) and the inner part made of P(NIPAAm-*co*-NIPMAAm), gelatin and gelatin methacrylate (GelMA). P(NIPAAm-*co*-NIPMAAm) was selected according to its thermal properties, which, together with gold nanorods (AuNRs), create an on-demand release system. The morphology of each layer of MS was investigated together with the chemical composition. A compression test was performed to discuss the mechanical properties of MS. NIR irradiation increased the temperature of samples and induced the detachment and release of the P(NIPAAm-*co*-NIPMAAm) layer. The photothermal effect activates bacterial eradication. The MS irradiated with NIR light killed *E. Coli* and *S. Aureus*, showing exceptional antimicrobial properties. This work presents the methodology for fabricating an adjustable system for the on-demand release of the hydrogel. By harnessing light-responsiveness, a new generation of nanostructured composites is being designed to accelerate the release and provide the desired properties of the material.

## 2. Results and Discussion

The MS for on-demand detachment and hydrogel release was manufactured using the multistep procedure. First, the polycarbonate (PC) mold was milled to fabricate the negative shape of the PDMS ring, which was molded in the next step. After curing with the temperature, the PDMS ring was modified with BP to crosslink the PDMS with the bottom layer of MS-GelMA. Then, the middle layer of gelatin and the top layer of P(NIPAAm-*co*-NIPMAAm) were prepared (**Figure 1**).

### 2.1. Physicochemical Properties

The structure of thermo-responsive MS was evaluated with field emission scanning electron microscopy (FE-SEM). Each layer is composed of an interconnected porous network with the pore size 14.89 ± 5.18, 9.46 ± 1.99, and 16.05 ± 6.91 µm, respectively, for P(NIPAAm-*co*-NIPMAAm), GelMA and gelatin (**Figure 2A–C**). These 3 materials are categorized as microporous hydrogels, facilitating the loading and release of drugs or other active agents and enhancing the diffusion of molecules.[43]

 

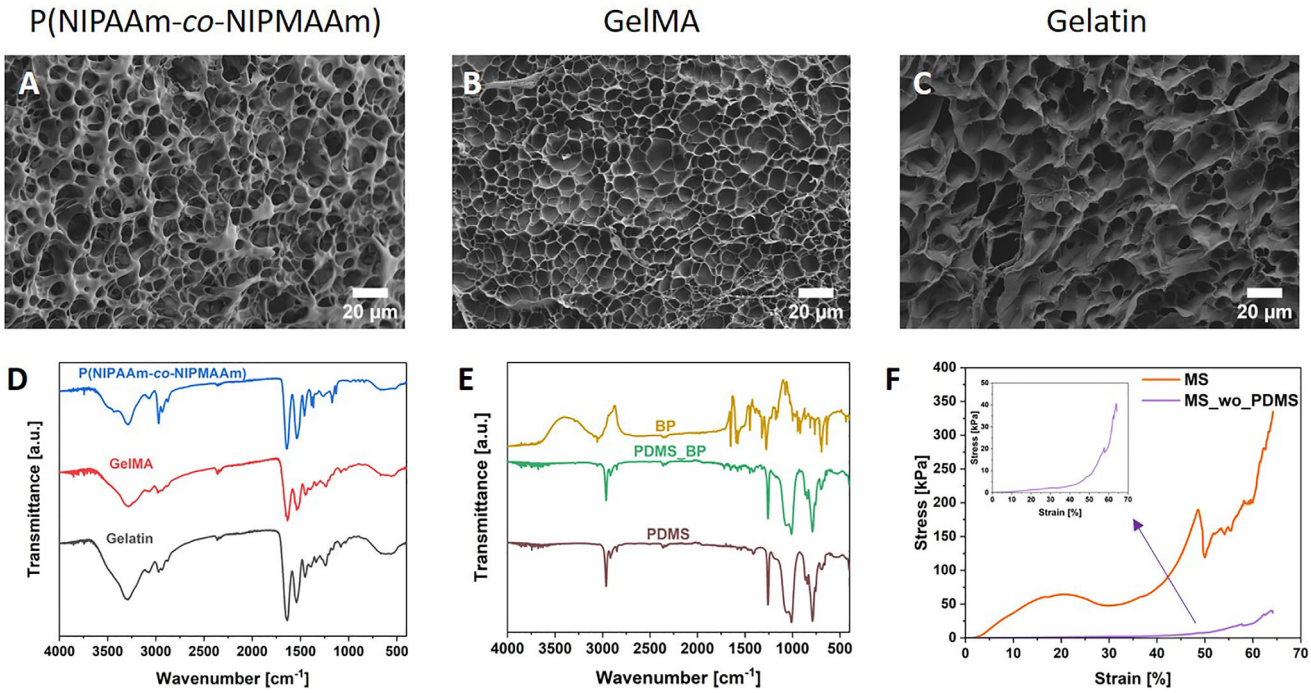


**Figure 2.** FE-SEM micrographs of the inner part of MS: A) P(NIPAAm-*co*-NIPMAAm); B) GelMA, and C) gelatin. D) FT-IR spectra of the inner part of MS and E) of the pristine PDMS ring and modified with BP. F) Representative compressive stress–strains curve of MS and MS without PDMS ring.

Gelatin has the most significant pore irregularity in shape and size (Figure 2C), while GelMA shows the greatest homogeneity (Figure 2B). The crosslinking of P(NIPAAm-*co*-NIPMAAm) and GelMA precursors provided more structure regularity than gelatin.[44] Further material characterization was performed with furier transform infrared spectroscopy (FT-IR; occurs Figure 2D,E). The spectra of each layer were similar, and the chemical composition of the used material was comparable. However, there are slight shifts within peak positions and differences in intensity. For P(NIPAAm-*co*-NIPMAAm), at 2969 and 2874 $cm^{-1}$, there are peaks related to the asymmetrical and symmetrical stretching of C—H. The stretching frequency of C═O appears at 1640 $cm^{-1}$.[45] The peak characteristic for amide bond is at 1539 $cm^{-1}$ for both GelMA and gelatin. The O—H stretching vibration frequency is at 3289 $cm^{-1}$ for gelatin, while for GelMA, it is slightly shifted to 3281 $cm^{-1}$. The peaks related to the N—H and C—H are located at 3071 and 2931 $cm^{-1}$, respectively.[46] For pristine PDMS, the asymmetric stretching of Si—O—Si is detected at 1059 and 1010 $cm^{-1}$, while the asymmetric stretching vibration of Si–$CH_3$ is at 787 $cm^{-1}$. In the spectra of PDMS modified with BP, those peaks remain almost unshifted, except 1059 $cm^{-1}$ moved to 1073 $cm^{-1}$ due to the modification with BP.[47,48] The C═C stretching vibration from the aromatic ring of benzophenone occurs between 1600–1400 $cm^{-1}$.[49]

Hydrogels are known for their low mechanical strength and being soft and flexible, for example, P(NIPAAm-*co*-NIPMAAm). Therefore, improvement of those properties would be beneficial for various applications.[50] Figure 2F shows representative compression–stress curves. To analyze the effect of PDMS on MS, the samples without PDMS (MS_wo_PDMS) were compressed. For this purpose, the PDMS ring was cut off from the samples, and the inner part was tested. The elastic modulus of MS was ≈60 times greater than for MS_wo_PDMS, reaching 425.5 ± 19.7 and 7.8 ± 1.1 kPa, respectively. Zheng and coworkers reached a similar level of magnitude of elastic modulus for pristine PNIPAAm.[51] Thus, ensuring that the PDMS ring enables MS manufacturing and maintains structural integrity.

### 2.2. Photothermal Characterization and On-Demand Release of Hydrogel

The photothermal effect of MS was investigated for various hydrogel precursor to AuNRs ratios and under different laser powers. The tested ratios were 2.5:1, 5:1, 7.5:1, and 10:1, while the evaluated laser power was 1, 1.5, 2, and 2.5 W $cm^{-2}$. The thermal response was possible (Figure S1A, Supporting Information), as AuNRs absorb energy in the NIR region and transfer it to the heat.[52] The time-temperature profile follows the same pattern regardless of the number of plasmonic particles incorporated into the hydrogel and laser power, showing a temperature increase proportional to the AuNRs amount and laser power. The more plasmonic particles were incorporated into the P(NIPAAm-*co*-NIPMAAm) hydrogel, and the higher laser power was used, the more the temperature increase was accelerated, reaching greater values (**Figure** 3A,B).[3] The correlation between the ΔT and both hydrogel precursor to AuNRs ratio and laser power was linear ($R^2$ = 0.990 and $R^2$ = 0.986, respectively); see Figure 3C,D. The optimization process of thermal response of MS was crucial to finding the balance between the AuNRs content, laser power, affecting the time of irradiation and reached temperature. The AuNRs triggered by the NIR light generated heat and

 

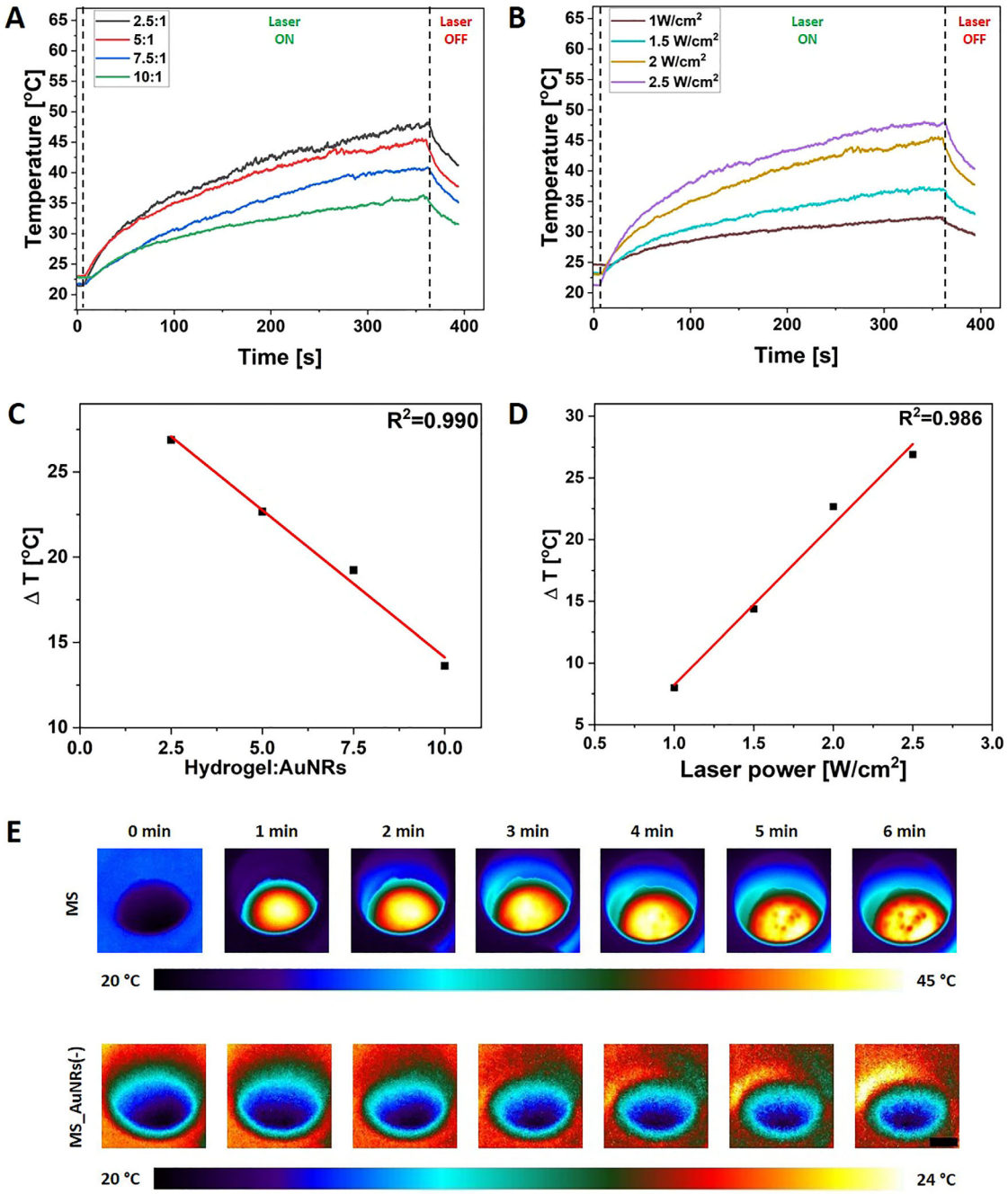


**Figure 3.** Photothermal optimization of the material. A) Temporal plots of different hydrogel precursor to AuNRs ratio–temperature dependence over time using constant laser power: 2 W $cm^{-2}$. B) Temporal plots of laser power–temperature dependence over time using constant hydrogel precursor to AuNRs ratio 5:1. C) Linear plot of hydrogel precursor to AuNRs ratio and ΔT dependence. D) Linear plot of laser power and ΔT dependence. E) Panel with thermal camera images showing the MS and control samples without the AuNRs (MS_AuNRs(–)) temperature before and after 1, 2, 3, 4, 5, and 6 min of laser irradiation. The scale bar is 5 mm.

locally increased the hydrogel temperature above VPTT, leading to the transition from hydrophilic to hydrophobic. Once the temperature exceeded 35 °C, the P(NIPAAm-*co*-NIPMAAm) matrix started shrinking, and gelatin was dissolved, enabling hydrogel release from the MS.[53,54] The hydrogel to AuNRs ratio equal to 5:1 and laser power to 2 W $cm^{-2}$ was selected as the most efficient for on-demand release, see Figure 3E. After 100 s of irradiation, the sample reached ≈35 °C (Figure 3A,B). Therefore, the releasing process started, reaching ≈45 °C within the next 260 s irradiation, and then the P(NIPAAm-*co*-NIPMAAm) hydrogel could be detached from the MS (Figure 3A,B,E; **Figures** 4A–D and S1A, Supporting Information). Moreover, when the sample without a gelatin layer was exposed to the NIR irradiation, the hydrogel release did not occur (Figure 4E–H); even

 

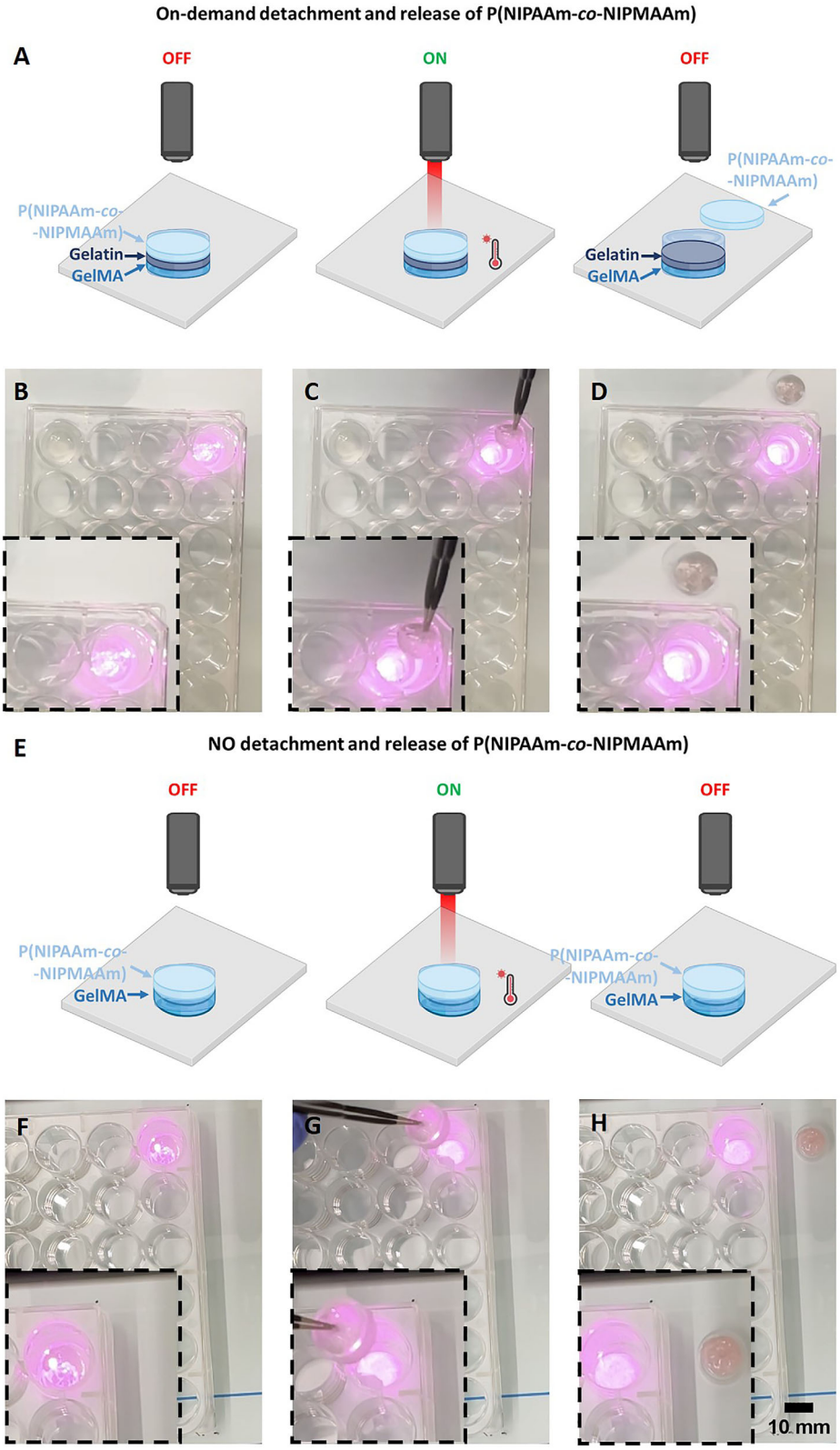


**Figure 4.** On-demand detachment and release of hydrogel from MS. A) Schematic of MS irradiated with NIR light; Images of MS in 24-well plate at B) beginning of irradiation, C) after 6 min of irradiation, and D) after the release of hydrogel (top layer of the MS). E) Schematic of MS without gelatin irradiated with NIR light; Images of MS in 24-well plate at F) beginning of irradiation, G) after 6 min of irradiation, and H) after sample removal from the well plate.

 

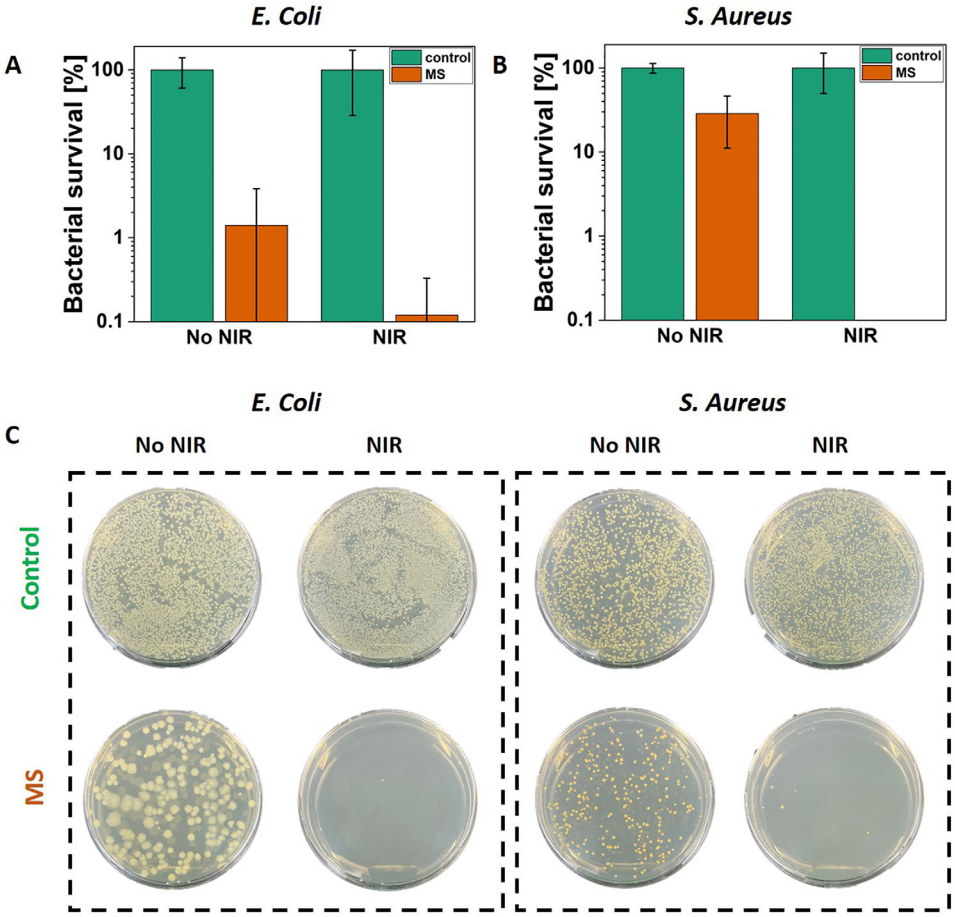


**Figure 5.** Photothermal inactivation of bacteria in contact with MS irradiated under NIR light. Survival percentage of A) *E. Coli* and B) *S. Aureus* in contact with the MS after 15 min of NIR irradiation or no irradiation. Bacteria suspension was used as a control. C) Images of representative plates of bacterial colonies grown on LB agar plates for each condition. Data are presented on a logarithmic scale as mean ± standard deviation.

the thermal effect remained unchanged (Figure S1B, Supporting Information). The BP was used as a crosslinker between the PDMS and GelMA.[55] The Schiff base reaction occurs between the P(NIPAAm-*co*-NIPMAAm) and GelMA during the sample processing.[56] Therefore, the gelatin was used as a middle layer of MS to create a barrier between the P(NIPAAm-*co*-NIPMAAm) and GelMA to block the bonding formation and enable the on-demand release of hydrogel (Figure 4A–D). These findings provide valuable insights for developing advanced materials with customizable photothermal response that enables hydrogel's controlled, on-demand release through precise laser irradiation.

### 2.3. Antibacterial Properties

The antibacterial properties of smart materials are essential for reducing the spread of pathogens. These materials can inhibit bacterial growth on surfaces, lowering the risk of contamination and reducing the need for chemical disinfectants. *E. Coli* and *S. Aureus*, representing gram-positive and gram-negative strains, were selected for verification of the pathogen eradication by the MS. Moreover, they are the most common strains for antibacterial studies. Plasmonic particles incorporated into the polymeric material and irradiated with the NIR enable local temperature increase, thus killing bacteria.[3,57–59] However, in the case of wet samples immersed in the bacteria suspension, the laser power has to be increased compared to the dry samples (Figure 3). After 15 min of irradiation with the contact with MS and reaching 59–62 °C, *E. Coli* growth was inactivated to 3 log units (the detection limit), showing only 0.1% of survived bacteria (n = 3, **Figure 5A**). The qualitative test of *S. Aureus* growth inhibition presented 100% killing of bacteria (n = 3, Figure 5B), while the obtained temperature was 56–61 °C. The representative plates of bacteria on MS after irradiation with NIR light demonstrate a few colonies (Figure 5C), confirming the antibacterial properties of MS. The slight difference between the qualitative and quantitative assays for *S. Aureus* in the case of MS irradiated with NIR may appear because the number of bacteria colonies to be detected was limited. The volume of bacterial suspension used for representative plates was greater than that used for the qualitative study. Thus, those four visible colonies could grow (Figure 5C). Moreover, bacteria growth was slightly reduced for the non-irradiated MS compared to the controls. This phenomenon is attributed to the BP

 

entrapped in the PDMS ring. The BP is able to target bacterial membranes, resulting in its depolarization. Therefore, it was used to synthesize benzophenone-based membrane-targeting antibiotics, effective even against MRSA (methicillin-resistant *Staphylococcus aureus*) and VRSA (vancomycin-resistant *Staphylococcus aureus*).[60,61] The significance of this study lies in demonstrating an innovative antibacterial strategy using plasmonic smart materials to effectively eliminate bacteria pathogens upon NIR irradiation.

## 3. Conclusion

This work described the development and characterization of the MS composed of P(NIPAAm-*co*-NIPMAAm), gelatin, and GelMA, with an on-demand hydrogel release with antibacterial properties. The production method is simple and based on the photo-crosslinking of P(NIPAAm-*co*-NIPMAAm) and GelMA precursors. Plasmonic nanoparticles incorporated into the top layer of MS induce a photothermal effect when the sample is exposed to NIR light. The heating performance increased within greater AuNRs to hydrogel ratio and higher laser power. Across different ratios between the plasmonic nanoparticles and hydrogel and laser power, the most efficient conditions for the on-demand hydrogel release from MS were selected.

The hydrogel to AuNRs ratio was set at 5:1, and laser power was equal to 2 W $cm^{-2}$. Within those parameters and 6 min of NIR irradiation, the P(NIPAAm-*co*-NIPMAAm) layer was released. Also, this work proved that the gelatin layer was essential for the on-demand detachment and release. The photothermal effect was efficient enough to kill 99.9% of *E. Coli* and 100% of *S. Aureus*, showing excellent antimicrobial properties of MS. Moreover, the antimicrobial effect was enhanced by the BP incorporated into the PDMS ring. The described study presents the material with tunable and bacterial eradication properties for the on-demand detachment and release of one of the MS layers, which could be used in soft robotics, optics, and actuators. This work introduces a novel material that, unlike most recent studies, facilitates the release of the whole part of MS, not only the active agents incorporated into the material matrix. In the future, more advanced systems will be manufactured using 3D printing for more precise design. Moreover, apart from plasmonic particles, short fibers or active agents could be incorporated into the hydrogel matrix to broaden the properties of materials and their application area.

## 4. Experimental Section

To prepare MS PDMS (Sylgard 184 Silicone Elastomer Kit, Dow Europe, Germany), gelatin type A (Sigma–Aldrich, Poland), phosphate buffered saline (PBS, pH ≈7.4, Sigma–Aldrich, Poland), methacrylic anhydride (2000 ppm topanol A as inhibitor, 94%, Carl Roth, Poland), 2-hydroxy-4′-(2-hydroxyethoxy)-2-methylpropiophenone (Igracure 2959, 98%, Sigma–Aldrich, Poland), gelatin from porcine skin (Sigma–Aldrich, Poland), N,N-isopropylacrylamide (NIPAAm, 97%, Sigma–Aldrich, Poland), N-isopropylmethacrylamide (NIPMAAm, 97%, Sigma–Aldrich, Poland), N,N′-methylene-*bis*-acrylamide (BIS-AAm, 99.5%, Carl Roth, Poland), gold nanorods (AuNRs, $\lambda a$ = 805 nm, O.D. = 50, AuNR ≈ 1 mg $mL^{-1}$, nanoComposix, USA), benzophenone (BP, 99%, Carl Roth, Poland), acetone (99%, Chemsolute, Th. Geyer, Poland), trichloro(1H, 1H, 2H, 2H-perfluorooctyl)silane (97%, Sigma–Aldrich, Poland) were used.

*GelMa Synthesis*: Gelatin was reacted with methacrylic anhydride to synthesize GelMA. Gelatin was dissolved in phosphate buffer (PBS; pH 7.5) at 50 °C to obtain 10% w/v solution. After the complete dissolution of the gelatin, 5 mL methacrylic anhydride was added dropwise under vigorous stirring and protected from the light. After 2 h of reaction, the mixture was diluted with 300 mL of warm PBS (37 °C), dialyzed (MWCO = 12 kDa) for 10 days against distilled water (DI) at room temperature, and finally freeze-dried.

*Preparation of GelMA and Gelatin Solution*: GelMA was dissolved in the DI water at 40 °C to obtain 6% w/v. Prior to adding the Irgacure 2959 to the GelMa solution, the stock solution was prepared by dissolving the photoinitiator at 10 mg $mL^{-1}$ in DI water at 70 °C. The Irgacure 2959 solution was added to the GelMA solution to obtain the final concentration of 0.05% w/v. Gelatin was dissolved in the DI water at 40 °C to obtain 2% w/v.

*Preparation of the Hydrogel Precursor Solution With AuNRs*: The hydrogel precursor solution (4.8% w/v) was prepared by mixing 578.1 mg of NIPAAm, 15.6 mg of NIPMAAm, 31.2 mg of BIS-AAm, 12.5 mg of Irgacure 2959 and dissolved in: 7.14, 8.33, 8.83, and 9.1 mL of DI water. A gold nanorod suspension, sonicated for 10 min, was added to the hydrogel precursor solution in a proportion of 1:2.5, 1:5, 1:7.5, and 1:10, and then the oxygen from the solution was removed using argon. For the control samples, the AuNRs suspension was substituted with water to keep the concentration of hydrogel components at the same level.

*Fabrication of Multilayered System*: MS for on-demand detachment and hydrogel release was manufactured using the multistep procedure. First, the mold was fabricated from 10 mm-thick polycarbonate (PC) plates (Macrolon, Bayer, Germany). The negative shape of the ring was milled into the plates using a CNC milling machine (Ergwind, Poland), which has a positioning reproducibility of 5 µm. A pressurized water washer was used to clean the surface of the mold from burrs or other contaminants. Then, it was silanized with 45 µL of trichloro(1H, 1H, 2H, 2H-perfluorooctyl)silane by placing the mold in the vacuum pump under 20 mbar (V-700, Buchi, Switzerland) for 12 min.

PDMS prepolymer and curing agent were mixed thoroughly in a ratio of 20:1, degassed under the vacuum, poured into the PC mold, and cured for 5 h at 80 °C. The PDMS ring was removed from the PC mold and immersed in the 10% w/v BP solution in acetone for 5 min to modify only the lower part of the ring. The PDMS ring was extensively washed with DI water and dried. Then, it was placed on the Petri Dish, 250 µL of 6% GelMa solution was added and crosslinked under a UV lamp (Dymax, 400 W, power density of 225 mW $cm^{-2}$) for 90 s. The second layer was prepared by adding 100 µL of 2% gelatin; then, the solution was solidified by storing it in the fridge (4 °C) for 20 min. Finally, 300 µL of P(NIPAAm-*co*-NIPMAAm) hydrogel with AuNRs was added and irradiated with a UV lamp for 140 s (in 7 intervals for 20 s). For the control, samples without AuNRs were prepared (Figure 1).

*Chemical and Morphological Analysis*: Before FT-IR and FE-SEM analysis, samples were frozen in liquid nitrogen and freeze-dried at −83 °C and 4.0 mbar (FreeZone Freeze Dryer, LABCONCO, USA).

Spectra of GelMA, gelatin, NIPAAm-*co*-NIPMAAm, BP, PDMS, and BP-modified PDMS were recorded on a Bruker Vertex70 FT-IR spectrometer in the ATR mode. Measurements were performed over the wavenumber range 4000–400 $cm^{-1}$, with a resolution of 1 $cm^{-1}$ and 10 scans per sample.

FE-SEM was performed with the ZEISS Crossbeam 350 FIB-SEM microscope. Before imaging, samples were sputtered with an ≈8 nm thick gold layer using a SC7620 Polaron mini sputter coater (Quorum Technologies Ltd, Ashford, UK).

*Compression Test*: Mechanical tests were conducted on the MS using CTX Texture Analyzer from Brookfield Ametek in compression mode. MS with a diameter of 13 mm and a height of 5.5 mm were manufactured and placed on a flat surface. MS without a PDMS ring was used as a control. The load cell of 5 kg was applied with a speed of 0.1 mm $s^{-1}$. Data acquisition occurred at a rate of 50 readings per second. The testing commenced when the load reached 0.1 N. Samples were compressed until destruction or maximum power.

*Photothermal Analysis*: The fiber-coupled laser (Coherent Powerline) with CW diode laser, operating at 808 nm, which was the high absorption

range of AuNRs, was used to stimulate the on-demand hydrogel release from an MS supplied with plasmonic nanoparticles. The thermal camera (FLIR, A655sc) with an accuracy of 0.2 °C, generating images with a resolution of 640 × 480 pixels, was used to capture the temperature profile under NIR irradiation. The thermal analysis of the MS was conducted in a dry state. Before selecting the final version of on-demand material, a diverse copolymer to AuNRs ratio (2.5:1, 5:1, 7.5:1, and 10:1) and laser power (1, 1.5, 2 and 2.5 W $cm^{-2}$) was tested. For this purpose, the dependence between the NIR laser power and ΔT was analyzed. Each sample was irradiated for 6 min in triplicates. Once the final material (copolymer to AuNRs ratio 5:1) was selected and laser power optimized (2 W $cm^{-2}$), the on-demand detachment of the hydrogel layer from the MS was performed.

*Antibacterial Properties*: Before microbial studies, samples were placed in the 24–well plates and sterilized under UV light for 30 min for each side. The antibacterial properties of MS were verified. *S. Aureus* (ATCC 6538) and *E. Coli* (ATCC 25 922) were isolated from culture with a streak plate method. A bacteria colony was isolated and inoculated in 3 mL of lysogeny broth (LB), and the suspension was incubated overnight in an orbital shaker at 37 °C. The next day, bacterial suspension was diluted in sterile PBS to obtain $10^6$ colony-forming units (CFU) $mL^{-1}$. Then, 500 µL of bacterial suspension was added to the samples and heated to 30 °C. Afterward, materials were exposed to NIR irradiation for 15 min. The laser power was set at 4.5 W $cm^{-2}$. The bacterial suspension was used as a positive control. For analyzing samples without irradiation, they were incubated at RT for 15 min. Next, 500 µL of sterile PBS was added to each well, and bacteria suspension was mixed; then, 100 µL of the solution was transferred to the 96–well plate and serially diluted and then plated on LB agar plates, which were incubated overnight at 37 °C. All the samples were tested in triplicates and with three technical repetitions. The bacterial survival was analyzed by counting the bacterial colonies. The plating technique limited the highest inactivation degree. It was detected at 3 log units of CFU $mL^{-1}$, allowing the detection of a survival rate of ≥0.1%.

For the qualitative study, the bacteria suspensions after contact with the materials were diluted 10 times, and 100 µL of this solution was spread evenly on representative LB agar plates. Plates were incubated overnight at 37 °C, and representative photos were captured the following day.

*Statistical Analysis*: The tests were performed at least in n ≥ 3 repetitions. All data were presented as mean ± standard deviation (SD).

## Supporting Information

Supporting Information is available from the Wiley Online Library or from the author.

## Acknowledgements

This work was supported by the National Science Centre (NCN) SONATA BIS Project No. 2020/38/E/ST5/00456. Figures 1 and 4 were partially created using BioRender.

## Conflict of Interest

The authors declare no conflict of interest.

## Data Availability Statement

The data that support the findings of this study are available from the corresponding author upon reasonable request.

## Keywords

antimicrobial properties, light-driven structural detachment, NIR light irradiation, plasmonic nanoparticles, smart hydrogel platform

Received: December 17, 2024
Revised: February 3, 2025
Published online: March 8, 2025

[1] S. S. Zargarian, B. Kupikowska-Stobba, A. Kosik-Kozioł, M. Bartolewska, A. Zakrzewska, D. Rybak, K. Bochenek, M. Osial, F. Pierini, *Mater. Today Chem.* **2024**, *41*, 102281.
[2] D. Yan, Z. Wang, Z. Zhang, *Acc. Chem. Res.* **2022**, *55*, 1047.
[3] D. Rybak, C. Rinoldi, P. Nakielski, J. Du, M. A. Haghighat Bayan, S. S. Zargarian, M. Pruchniewski, X. Li, B. Strojny-Cieślak, B. Ding, F. Pierini, *J. Mater. Chem. B* **2024**, *12*, 1905.
[4] S. Dai, P. Ravi, K. C. Tam, *Soft Matter* **2008**, *4*, 435.
[5] J. He, Q. Zhou, Z. Ge, S. Jiang, J. Li, W. Feng, H. Yang, *Adv. Funct. Mater.* **2024**, 2403341.
[6] Y. Itoh, D. Morishita, *Polym. J.* **2023**, *55*, 1035.
[7] G. Uğur, J. Chang, S. Xiang, L. Lin, J. Lu, *Adv. Mater.* **2012**, *24*, 2685.
[8] X. Hou, Y. Zhou, Y. Liu, L. Wang, J. Wang, *J. Mater. Sci.* **2020**, *55*, 16033.
[9] G. Priniotakis, U. Stachewicz, J. van Hoof, *Indoor Built Environ.* **2022**, *31*, 1443.
[10] X. Wang, H. Hu, Z. Yang, L. He, Y. Kong, B. Fei, J. H. Xin, *Smart Mater. Struct.* **2014**, *23*, 125027.
[11] Z. J. Krysiak, U. Stachewicz, *Wiley Interdiscip. Rev. Nanomed. Nanobiotechnol.* **2023**, *15*, e1829.
[12] V. K. Srivastava, P. K. Jain, P. Kumar, A. Pegoretti, C. R. Bowen, *J. Mater. Eng. Perform.* **2020**, *29*, 4162.
[13] X. Yu, H. Cheng, M. Zhang, Y. Zhao, L. Qu, G. Shi, *Nat. Rev. Mater.* **2017**, *2*, 17046.
[14] N. Rajabi, M. Kharaziha, R. Emadi, A. Zarrabi, H. Mokhtari, S. Salehi, *J. Colloid Interface Sci.* **2020**, *564*, 155.
[15] L. Zhang, B. Luo, Z. An, P. Zheng, Y. Liu, H. Zhao, Z. Zhang, T. Gao, Y. Cao, Y. Zhang, R. Pei, *Biomacromolecules* **2023**, *24*, 5769.
[16] H. Sun, J. Chen, X. Han, H. Liu, *Mater. Sci. Eng. C* **2018**, *82*, 284.
[17] M. A. Ward, T. K. Georgiou, *Polymers (Basel)* **2011**, *3*, 1215.
[18] M. Xia, Y. Cheng, Z. Meng, X. Jiang, Z. Chen, P. Theato, M. Zhu, *Macromol. Rapid Commun.* **2015**, *36*, 477.
[19] W. Du, S. Sun, Z. Zhao, B. Zhao, X. Zhang, *Mater. Horiz.* **2024**, *12*, 597.
[20] M. K. Kokufuta, S. Sato, E. Kokufuta, *Colloid Polym. Sci.* **2012**, *290*, 1671.
[21] E. Díez-Peña, I. Quijada-Garrido, P. Frutos, J. Barrales-Rienda, *Macromolecules* **2002**, *35*, 2667.
[22] Z. Chen, Y. Chen, C. Chen, X. Zheng, H. Li, H. Liu, *Chem. Eng. J.* **2021**, *424*, 130462.
[23] S. Pawłowska, C. Rinoldi, P. Nakielski, Y. Ziai, O. Urbanek, X. Li, T. A. Kowalewski, B. Ding, F. Pierini, *Adv. Mater. Interfaces* **2020**, *7*, 2000247.
[24] Y. Pei, J. Chen, L. Yang, L. Shi, Q. Tao, B. Hui, J. Li, *J. Biomater. Sci., Polym. Ed.* **2004**, *15*, 585.
[25] J. P. Monteiro, S. M. Predabon, C. T. P. Da Silva, E. Radovanovic, E. M. Girotto, *J. Appl. Polym. Sci.* **2015**, *132*, 1.
[26] F. Pierini, P. Nakielski, O. Urbanek, S. Pawlowska, M. Lanzi, L. De Sio, T. A. Kowalewski, *Biomacromolecules* **2018**, *19*, 4147.
[27] J. L. Li, M. Gu, *Biomaterials* **2010**, *31*, 9492.
[28] D. Rybak, J. Du, P. Nakielski, C. Rinoldi, A. Kosik-Kozioł, A. Zakrzewska, H. Wu, J. Li, X. Li, Y. Yu, B. Ding, F. Pierini, *Adv. Healthcare Mater.* **2024**, *2404274*, 2404274.
[29] J. E. Won, T. I. Wi, C. M. Lee, J. H. Lee, T. H. Kang, J. W. Lee, B. C. Shin, Y. J. Lee, Y. M. Park, H. D. Han, *Acta Biomater.* **2021**, *136*, 508.
[30] G. Gao, Y. W. Jiang, H. R. Jia, F. G. Wu, *Biomaterials* **2019**, *188*, 83.
[31] I. Matai, G. Kaur, S. Soni, A. Sachdev, Vikas, S. M., *J. Photochem. Photobiol. B Biol.* **2020**, *210*, 111960 .

 

[32] C. Zhao, B. Pan, T. Wang, H. Yang, D. Vance, X. Li, H. Zhao, X. Hu, T. Yang, Z. Chen, L. Hao, T. Liu, Y. Wang, *Pharmaceutics* **2023**, *15*, 2729.
[33] S. T. Yohe, Y. L. Colson, M. W. Grinstaff, *J. Am. Chem. Soc.* **2012**, *134*, 2016.
[34] S. F. Chou, D. Carson, K. A. Woodrow, *J. Controlled Release* **2015**, *220*, 584.
[35] D. Han, A. J. Steckl, *ACS Appl. Mater. Interfaces* **2013**, *5*, 8241.
[36] H. Chen, J. Xu, Y. Jiang, J. Sun, W. Zheng, H. Qian, J. Sun, W. Hu, *Small*, *n/a*, 2410566.
[37] Y. Chen, B. Gu, X. Hao, Z. Lu, D. Wang, *J. Colloid Interface Sci.* **2025**, *680*, 172.
[38] S. Ida, T. Hikida, A. Kawai, T. Matsuda, S. Suzuki, H. Imoto, K. Naka, S. Kanaoka, *Polym. Chem.* **2023**, *14*, 2771.
[39] Q. Zhang, C. Weber, U. S. Schubert, R. Hoogenboom, *Mater. Horiz.* **2017**, *4*, 109.
[40] P. Tallury, R. Airrabeelli, J. Li, D. Paquette, S. Kalachandra, *Dent. Mater.* **2008**, *24*, 274.
[41] G. Verreck, I. Chun, J. Rosenblatt, J. Peeters, A. Van Dijck, J. Mensch, M. Noppe, M. E. Brewster, *J. Controlled Release* **2003**, *92*, 349.
[42] F. Pierini, A. Guglielmelli, O. Urbanek, P. Nakielski, L. Pezzi, R. Buda, M. Lanzi, T. A. Kowalewski, L. De Sio, *Adv. Opt. Mater.* **2020**, *8*, 2000324.
[43] N. H. Thang, T. B. Chien, D. X. Cuong, *Gels* **2023**, *9*, 523.
[44] T. Kopač, A. Ručigaj, M. Krajnc, *Int. J. Biol. Macromol.* **2020**, *159*, 557.
[45] Y. Ziai, M. Lanzi, C. Rinoldi, S. S. Zargarian, A. Zakrzewska, A. Kosik-Kozioł, P. Nakielski, F. Pierini, *Nanoscale Adv* **2024**, *6*, 1246.
[46] E. Jamshidifar, M. Esfandyari-Manesh, H. Motasadizadeh, S. Naderizadeh, A. Yourdkhani, N. Samadi, R. Dinarvand, *J. Mater. Sci.* **2022**, *57*, 13603.
[47] T. Lei, Y. Zhao, X. Zhai, S. Ji, B. Song, W. Dong, C. Teng, W. Wei, *Mater. Des.* **2023**, *229*, 111915.
[48] J. Lee, J. Kim, H. Kim, Y. M. Bae, K. H. Lee, H. J. Cho, *J. Micromechanics Microengineering* **2013**, *23*, 3.
[49] K. Sankaranarayanan, P. Ramasamy, *J. Cryst. Growth* **2005**, *280*, 467.
[50] Q. Wang, T. A. Asoh, H. Uyama, *RSC Adv.* **2018**, *8*, 12608.
[51] W. J. Zheng, N. An, J. H. Yang, J. Zhou, Y. M. Chen, *ACS Appl. Mater. Interfaces* **2015**, *7*, 1758.
[52] X. Luo, L. Du, Z. Wen, W. Lv, F. Zhao, X. Jiang, Y. Peng, L. Sun, Y. Li, J. Rao, *Nanoscale* **2015**, *7*, 14422.
[53] P. Nakielski, S. Pawłowska, C. Rinoldi, Y. Ziai, L. De Sio, O. Urbanek, K. Zembrzycki, M. Pruchniewski, M. Lanzi, E. Salatelli, A. Calogero, T. A. Kowalewski, A. L. Yarin, F. Pierini, *ACS Appl. Mater. Interfaces* **2020**, *12*, 54328.
[54] D. L. Kramer, *Encycl. Mater. Sci. Technol.* **2001**, 3495.
[55] D. Keskin, T. Mokabbar, Y. Pei, P. van Rijn, *Polymers (Basel)* **2018**, *10*, 534.
[56] K. Karakyriazis, V. Lührs, S. Stößlein, I. Grunwald, A. Hartwig, *Mater. Adv* **2023**, *4*, 1648.
[57] M. A. Haghighat Bayan, C. Rinoldi, A. Kosik-Kozioł, M. Bartolewska, D. Rybak, S. S. Zargarian, S. A. Shah, Z. J. Krysiak, S. Zhang, M. Lanzi, P. Nakielski, B. Ding, F. Pierini, *Adv. Mater. Technol.* **2024**, *10*, 2400450.
[58] M. Bartolewska, A. Kosik-Kozioł, Z. Korwek, Z. Krysiak, D. Montroni, M. Mazur, G. Falini, F. Pierini, *Adv. Healthcare Mater.* **2024**, *14*, 2402431.
[59] T. Yang, D. Wang, X. Liu, *Colloids Surf., B* **2019**, *173*, 833.
[60] S. K. Vooturi, M. B. Dewal, S. M. Firestine, *Org. Biomol. Chem.* **2011**, *9*, 6367.
[61] S. K. Vooturi, C. M. Cheung, M. J. Rybak, S. M. Firestine, *J. Med. Chem.* **2009**, *52*, 5020.

 